NeuroImage 60 (2012) 117–129

Contents lists available at SciVerse ScienceDirect

NeuroImage

journal homepage: www.elsevier.com/locate/ynimg

Cognitive: Executive Function

# The functional connectivity of the human caudate: An application of meta-analytic connectivity modeling with behavioral filtering

Jennifer L. Robinson [a,b,c,d,*], Angela R. Laird [c], David C. Glahn [e], John Blangero [f], Manjit K. Sanghera [a], Luiz Pessoa [g], P. Mickle Fox [c], Angela Uecker [c], Gerhard Friehs [a], Keith A. Young [b,d], Jennifer L. Griffin [b,d], William R. Lovallo [h], Peter T. Fox [c]

[a] Neuroscience Institute, Scott & White Healthcare, Texas A&M Health Science Center, College of Medicine, Temple, TX, USA
[b] VISN 17 Center of Excellence for Research on Returning War Veterans, Central Texas Veterans Health Care System, Waco, TX, USA
[c] Research Imaging Institute, University of Texas Health Science Center at San Antonio, San Antonio, TX, USA
[d] Texas A&M Health Science Center, College of Medicine, Department of Psychiatry and Behavioral Science, Temple, TX, USA
[e] Olin Neuropsychiatric Research Center, Institute of Living and Yale University, Department of Psychiatry, New Haven, CT, USA
[f] University of Texas Health Science Center, Department of Genetics, Texas Biomedical Research Institute, San Antonio, TX, USA
[g] Department of Psychology, University of Maryland, College Park, MD, USA
[h] Behavioral Sciences Laboratories, Veterans Affairs Medical Center, Oklahoma City, Oklahoma, USA

ARTICLE INFO

*Article history:*
Received 6 September 2011
Revised 30 November 2011
Accepted 6 December 2011
Available online 14 December 2011

*Keywords:*
Meta-analytic connectivity modeling
Functional connectivity
MACM
DTI
Caudate

ABSTRACT

Meta-analysis based techniques are emerging as powerful, robust tools for developing models of connectivity in functional neuroimaging. Here, we apply meta-analytic connectivity modeling to the human caudate to 1) develop a model of functional connectivity, 2) determine if meta-analytic methods are sufficiently sensitive to detect behavioral domain specificity within region-specific functional connectivity networks, and 3) compare meta-analytic driven segmentation to structural connectivity parcellation using diffusion tensor imaging. Results demonstrate strong coherence between meta-analytic and data-driven methods. Specifically, we found that behavioral filtering resulted in cognition and emotion related structures and networks primarily localized to the head of the caudate nucleus, while perceptual and action specific regions localized to the body of the caudate, consistent with early models of nonhuman primate histological studies and postmortem studies in humans. Diffusion tensor imaging (DTI) revealed support for meta-analytic connectivity modeling's (MACM) utility in identifying both direct and indirect connectivity. Our results provide further validation of meta-analytic connectivity modeling, while also highlighting an additional potential, namely the extraction of behavioral domain specific functional connectivity.

Published by Elsevier Inc.

## Introduction

The human dorsal striatum contains the primary input to the basal ganglia (Grahn et al., 2008; Haber, 2003). Composed of the caudate and putamen, it receives axons from all regions of the cortex with the exception of the primary visual, auditory, and olfactory cortices (Grahn et al., 2008). Anatomical, functional, and/or connectivity abnormalities of the caudate nuclei have been noted in a wide range of disorders including autism (Turner et al., 2006), Huntington's disease (Bohanna et al., 2011), Parkinson's disease (PD) (Rowe et al., 2008), human immunodeficiency virus (HIV) (Melrose et al., 2008), drug addiction (Ma et al., 2011), depression (Bluhm et al., 2009), and attention deficit hyperactivity disorder (ADHD) (Casey et al., 2007). Despite its involvement in a range of psychiatric and neurological disorders, few studies have examined the functional connectivity of the human caudate (Di Martino et al., 2008; Postuma and Dagher, 2006), and no study, to our knowledge, has examined functional connectivity in this structure using advanced meta-analytic techniques. In the present study, we used meta-analytic connectivity modeling (MACM) (Robinson et al., 2010) to provide an initial model of functional connectivity utilizing decades worth of neuroimaging data collected across various behavioral domains. Describing connectivity models in this manner has the potential to facilitate discovery of specific pathways that are aberrant in populations with known dysfunction of the caudate, which may ultimately lead to the identification of novel interventions.

Early models of the basal ganglia assigned to the caudate a primary role of integrating information from the cortical association and sensorimotor areas of the brain before sending it to distinct ventrolateral thalamic sub-regions, which would then relay the information almost exclusively to the primary motor cortex. These early models have largely been replaced by more complex ones based on evidence

* Corresponding author at: Scott & White Memorial Hospital, Neuroscience Institute, 2401 S. 31st Street, Temple, TX 76508. Fax: +1 254 724 6332.
*E-mail address:* jrobinson@swmail.sw.org (J.L. Robinson).

1053-8119/$ – see front matter. Published by Elsevier Inc.
doi:10.1016/j.neuroimage.2011.12.010

of reciprocating but interconnected circuits that link the cortex, basal ganglia, and thalamus (Alexander and Crutcher, 1990; Alexander et al., 1986; DeLong et al., 1983). Five primary circuits have been proposed in the nonhuman primate literature: motor, oculomotor, dorsolateral prefrontal, lateral orbitofrontal, and anterior cingulate (Alexander et al., 1986). In each of these proposed circuits, the basal ganglia receive input from multiple cortical regions, pass this information to the thalamus where integration operations occur before information is passed to specific cortical regions of one of the segregated functional circuits (Alexander et al., 1986). Thus, each cycle within a thalamocortical-basal ganglia circuit concludes with the thalamocortical pathway terminating in specific regions of the cortex, unique to that particular loop. To date, these looping circuits have not been adequately described in human functional neuroimaging studies.

Topographic mapping within the caudate has been demonstrated in animal models. Specifically, segmentation of the caudate nucleus into head and body components has revealed consistent, distinct compartments such that the head of the caudate has been associated with more cognitive and emotional processing whereas the body/tail of the caudate has been associated with action and perceptual processes. However, similar to the proposed looping circuits, no study to our knowledge has tested this organization in humans.

Here, we test whether the human caudate connectivity patterns support the major circuits identified in the nonhuman primate system, and investigate whether it demonstrates anterior–posterior somatotopic and behavioral topography. Because it is not feasible to investigate this in a single study, we capitalize on the power of meta-analyses and the organization of the BrainMap database (Fox and Lancaster, 2002; Fox et al., 2005; Laird et al., 2005b) database to 1) identify behavioral domain-specific networks that we predict will correspond to the circuits described in the primate literature, and 2) determine if the anterior and posterior portions of the caudate demonstrate behavioral domain segmentation as previously described with action and perception networks mapping primarily to the posterior body/tail of the caudate, and cognitive and emotional systems relying on more anterior aspects of the structure. To do so, we use a robust, unbiased meta-analytic approach, coupled with a tractography analysis using diffusion tensor imaging (DTI).

## Methods

Meta-analytic connectivity modeling (MACM) was employed to assess human caudate functional connectivity. Below, we describe methods for region of interest (ROI) selection as well as the implementation of MACM.

### *ROI selection*

Bilateral caudate ROIs were defined using the Harvard-Oxford Structural Probability Atlas (thresholded at 75% probability) distributed with FSL neuroimaging analysis software (http://www.fmrib.ox.ac.uk/fsl/fslview/atlas-descriptions.html#ho) (Smith et al., 2004). Using anatomically bounded (i.e., irregular) ROIs represents an improvement over methodologies which use regular (i.e., spherical or cuboidal) ROIs (Stein et al., 2007), ROIs derived from functional activations within a given study (Gianaros et al., 2008; Mohanty et al., 2007), or use atlas-based automatic labeling systems (Tzourio-Mazoyer et al., 2002; Williams et al., 2006). The mean probability for the left (M ± SD: 87.82% ± 6.87%) and right caudate (88.20% ± 7.18%) was over 85%, and the centroid for each had over 95% (left: 96% at Talairach coordinates [x,y,z] −11.2, 6.6, 11.6; right: 98% at Talairach coordinates 13.2, 7.5, 12.0) probability of being part of the caudate. The total volume for the left caudate was 1635 voxels, and the right caudate was 1845 voxels. For additional analyses, we generated a head and body caudate ROI.

### *Caudate head and body ROIs*

Given that cytoarchitectural, histological, and early neuroimaging studies suggested a behavioral domain segmentation of the caudate, such that the head of the caudate was thought to be involved in more cognition and emotion related processes, while the body/tail was involved primarily with action and perception, we manually divided the caudate ROI into head and body subsections based on previous research (Castellanos et al., 1994; Williams et al., 1989). Specifically, we designated the boundary between the head and body of the caudate to be the coronal slice containing the interventricular foramina. The bilateral caudate head ROI was 1677 voxels (left, 731 voxels centered at −15, 10, 17; right 946 voxels centered at 15, 9, 19). The bilateral caudate body ROI was 1803 voxels (left, 904 voxels centered at −14, −4, 23; right, 899 voxels centered at 17, −10, 24).

### *BrainMap meta-analysis methods*

To search for all studies that reported activation within each ROI boundary, the left and right caudate ROIs were input into the BrainMap database separately, with restrictions to exclude disease-based studies, and include only activation studies. Whole-brain coordinates of activations from the isolated contrasts were then downloaded (left caudate = 125 papers, 167 experiments, 2466 locations; right caudate = 135 papers, 200 experiments, 2907 locations). The total number of subjects in all studies reporting activation in the left caudate was 2094, and for the right caudate 2136. Papers were drawn from all of the behavioral domains coded in the BrainMap database which includes cognition, emotion, action, interoception, pharmacology, and perception, with cognition representing the majority of studies followed by emotion for both the left and right caudate. For more detailed information regarding the taxonomy and coding strategy of the BrainMap database, please refer to Fox et al. (2005), Laird et al. (2009a, 2011a) and the BrainMap lexicon located at http://www.brainmap.org/BrainMapLex.xls. Of the final data set, 48% of the papers drawn for the left caudate were coded as cognition, 24% as emotion, 13% as perception,10% as action, 3% as pharmacology, and 1% as interoception. For the right caudate, 44% were coded as cognition, 25% as emotion, 15% as action, 12% as perception, 2% as interoception, and 2% as pharmacology.

Activation likelihood estimation (ALE) meta-analyses (Laird et al., 2005a,b; Turkeltaub et al., 2002, 2012) were performed on the sets of coordinates identified as coactivated during left and right caudate activation, to identify regions of convergence. This map served as a 'global' connectivity map, encompassing all behavioral domains. ALE capitalizes on the nature of voxel-wise studies that are commonly reported in a standard stereotactic space ($x$, $y$, $z$) by pooling 3D coordinates from like studies, and providing the probability of an event occurring at each brain voxel. Resultant ALE maps from the present study were thresholded conservatively ($p<0.001$, corrected for multiple comparisons via false discovery rate, with minimum cluster volume 100 $mm^3$).

### *Head versus body MACM functional connectivity*

The caudate head and body ROIs were input into the BrainMap database and subsequent functional connectivity maps were created based on the resultant ALE analyses, as described above. Ninety-one papers with caudate head activation were drawn from the database (1300 subjects, 109 experiments, 245 conditions, 1709 locations), and 115 papers were drawn for the body/tail of the caudate (1972 subjects, 141 experiments, 304 conditions, 2210 locations).

### *Behavioral domain-specific MACM functional connectivity*

The above BrainMap search results for the left and right caudate ROIs were then restricted to the major behavioral domain categories, and the whole-brain ALE meta-analyses were repeated separately for each ROI, for each domain (e.g., action, cognition, emotion, interoception, pharmacology, and perception). The behavioral domain datasets

varied in size (action: 51 papers drawn from the database, representing 777 subjects, 109 experiments, 146 conditions, and 1481 locations; cognition: 151 papers, 2370 subjects, 354 experiments, 501 conditions, 4421 locations; emotion: 72 papers, 1269 subjects, 201 experiments, 290 conditions, 1908 locations; perception: 54 papers, 711 subjects, 95 experiments, 137 conditions, 1606 locations). Interoception and pharmacology were not included in the analysis because they had 6 and 9 papers, respectively. Resultant ALE maps were generated for each behavioral domain with sufficient power. To identify regions of coactivation specific to a given behavioral domain, all other behavioral domain specific connectivity maps except the domain of interest were subtracted from the global functional connectivity map leaving only coactivations that were not involved in any other domain's functional connectivity map.

*Structural segmentation methods*

Motivated by prior evidence from nonhuman primates and human neuroimaging studies, we performed a diffusion tensor imaging analysis to probe structural segmentation. Diffusion-weighted data were acquired on forty-nine healthy, Hispanic individuals (age: 40.94 years ± 8.38; education: 12.47 years ± 2.69; 16 males, 33 females) who were recruited into an Institution Review Board approved neuroimaging study at the University of Texas Health Science Center at San Antonio, Research Imaging Institute. All individuals included in the analysis were screened for psychiatric illness and neurological conditions, and had never lost consciousness. Data were acquired on a Siemens 3 T scanner with a standard 8-channel headcoil. Diffusion weighting was isotropically distributed along 55 directions ($b$-value = 0, 700; TR/TE = 7800/88 ms, base resolution = 128 mm, voxel size = 1.72 mm × 1.72 mm × 3 mm; 50 slices acquired; total scan time = 7 min40 sec). In each subject, a high-resolution $T_1$-weighted scan was obtained for registration purposes (MPRAGE, TR/TE = 2200/3.04 ms, tip angle = 13°, voxel size = 0.8 $mm^3$, 208 slices, base resolution = 320 mm, FOV Phase = 70%, FOV Read = 256 mm). All images (diffusion-weighted and $T_1$-weighted) were skull-stripped using tools provided in FSL (Smith, 2002), and manually checked to ensure accuracy.

*Image analysis*

Probabilistic diffusion tractography was carried out as described previously (Behrens et al., 2003a,b; Johansen-Berg et al., 2005). In summary, a probability density function was created at each voxel on the principal fiber direction. Connectivity probabilities were estimated between the seed voxels and target voxels by repeatedly sampling connected pathways through the probability distribution function. We used the same anatomically defined bilateral caudate ROIs as described previously as our seed masks, and 11 cortical and subcortical regions covering the whole brain as targets. All targets were generated using the Harvard-Oxford probability atlas and included the following regions: anterior cingulate, paracingulate, prefrontal cortex, precentral gyrus, postcentral gyrus, parietal lobe, temporal lobe, occipital lobe, posterior cingulate, amygdala and hippocampus. All target ROIs were thresholded at 50% probability with the exception of the amygdala and hippocampus, which were more conservatively thresholded (70%). Target ROIs were transformed into each subject's space using registration tools provided in FSL (Jenkinson et al., 2002).

From each voxel in the caudate mask, samples were drawn from the connectivity distribution and the proportion of those samples that passed through each of the cortical/subcortical masks was defined as the probability of connection to the target. Segmentation of the caudate was performed by classifying each seed voxel as connecting to the cortical or subcortical mask with the highest connectivity probability. For each target, we thresholded and binarized individual subject results to include only those caudate voxels with a connection probability > 10%. These images were combined to create group probability maps of caudate sub-regions.

Finally, as proof of concept of MACM's potential to identify both direct and indirect connectivity, we manually created ROIs by drawing a 5 mm sphere around the centers of each cluster of the resultant whole database ALE maps of the right and left caudate. We chose spheres over anatomical ROIs since we had evidence to support the location of the focus within each cluster, and since those clusters did not encompass the entire anatomical location of the focus. Additionally, we chose to use a spherical ROI because some of the clusters had multiple foci. Therefore, we wanted to capture the independent contribution of each of these foci without getting into shared contribution issues. These were used as targets in a probabilistic tractography analysis with the right and left caudate as seeds, respectively. The same analysis was carried out as with the 11 atlas defined targets described above.

## Results

*Modeling of functional connectivity*

We observed significant functional connectivity of both the left and right caudate to regions of the left anterior (BA32) and posterior cingulate (BA23), left and right insula (BA13), thalamus (medial dorsal nucleus), and inferior frontal gyrus (BA9), and left middle frontal (BA6) and precentral gyri (Table 1). In addition, we found multiple regions of functional connectivity that were spatially distinct with different Talairach Daemon labels between the right and left caudate maps. Specifically, for the left caudate, we found additional regions of coactivation with the left middle frontal gyrus (BA10), the right middle frontal gyrus, and left inferior frontal gyrus (BA9/46), regions that have been implicated in emotional and cognitive processing. We also found co-activation among the left posterior cingulate gyrus (BA23/31) and anterior cingulate (BA24), as well as the right parahippocampal gyrus (BA27) and hippocampus. Additionally, we found evidence for functional connectivity among the right precentral gyrus, known for its association with motor planning, in addition to the left postcentral gyrus. We found functional connectivity to the left inferior occipital gyrus (BA19), the left fusiform gyrus (BA37), and the left and right parietal lobules. The right caudate showed functional connectivity differences to regions of the left (BA9) and right (BA6) middle frontal gyrus, as well as the left medial frontal gyrus (BA6) and bilateral cingulate (BA32). We found further deviations between functional connectivity between hemispheres with regard to the right thalamus (pulvinar) and right lentiform nucleus (lateral globus pallidus) as well. ALE results are displayed in Fig. 1. Differences between hemispheres were based on Talairach Daemon labels as well as proximity of coordinates.

*Behavioral domain classification*

One of the advantages to assessing the functional connectivity of a given region using MACM is the opportunity to mine the behavioral domain classification of metadata embedded in the BrainMap database. This additional information allows for the examination of behavioral domains associated with the ALE results to determine if the frequency of domain 'hits' relative to the distribution across the entire database are significantly different (Laird et al., 2009b). We performed a $\chi^2$ test on the distribution of papers from a search of bilateral caudate ROIs. If the distributions were significantly different from the database, a binomial test was performed to determine which individual domains were over- or under-represented. For the bilateral caudate search, higher than expected frequencies were identified for pharmacology ($p<0.0004$) and emotion ($p<0.0001$), and a lower than expected frequency distribution was noted for perception ($p<0.0001$). Individual caudate analyses (left caudate only and right caudate only) using the same analysis strategy demonstrated higher than expected distributions for emotion ($p<0.0001$).

**Table 1**
ALE meta-analyses on the right and left caudate demonstrated overlapping regions of functional connectivity (top portion of table) as well as spatially distinct differences as determined by a qualitative label and coordinate based review. Results were thresholded at the $p<0.001$ level.

| Lobe | Region | BA | Left caudate connectivity | | | | Right caudate connectivity | | | |
|---|---|---|---|---|---|---|---|---|---|---|
| | | | ALE | x | y | z | ALE | x | y | z |
| *Clusters shared for both left and right caudate connectivity analyses* | | | | | | | | | | |
| Frontal | Left middle frontal gyrus | 6 | 0.107 | −26 | −10 | 56 | 0.064 | −38 | −4 | 44 |
| | | | 0.081 | −28 | 10 | 46 | | | | |
| | Left precentral gyrus | | 0.106 | −40 | −4 | 44 | 0.045 | −30 | −12 | 56 |
| | Left inferior frontal gyrus | 9 | 0.163 | −46 | 10 | 28 | 0.065 | −50 | 6 | 30 |
| | Right inferior frontal gyrus | | 0.109 | 42 | 4 | 30 | 0.056 | 42 | 8 | 32 |
| Limbic | Left posterior cingulate | 23 | 0.085 | −2 | −52 | 20 | 0.049 | −2 | −54 | 20 |
| | Left anterior cingulate | 32 | 0.082 | −2 | 46 | −2 | 0.038 | −4 | 36 | 12 |
| Sub-lobar | Left insula | 13 | 0.237 | −32 | 18 | 4 | 0.151 | −32 | 18 | 6 |
| | | | 0.077 | −46 | −22 | 14 | | | | |
| | Right insula | | 0.211 | 34 | 18 | 4 | 0.160 | 32 | 20 | 4 |
| | Left caudate | Caudate head | 0.358 | −10 | 8 | 4 | 0.197 | −12 | 8 | 4 |
| | Left Thalamus | Medial dorsal nucleus | 0.215 | −12 | −18 | 8 | 0.134 | −10 | −18 | 10 |
| | Right thalamus | Medial dorsal nucleus | 0.168 | 10 | −12 | 10 | 0.111 | 8 | −14 | 10 |
| *Hemisphere specific clusters based on visual comparison* | | | | | | | | | | |
| Anterior frontal | Right dentate | Dentate | 0.104 | 18 | −54 | −22 | | | | |
| | Left middle frontal gyrus | 10 | 0.087 | −34 | 42 | 18 | | | | |
| | | 6 | 0.100 | −24 | −4 | 50 | | | | |
| | Right middle frontal gyrus | 9 | 0.092 | 40 | 30 | 32 | | | | |
| | | 46 | 0.105 | 42 | 28 | 18 | | | | |
| | Left inferior frontal gyrus | 46 | 0.070 | −44 | 42 | 4 | | | | |
| | Right inferior frontal gyrus | 9 | 0.106 | 48 | 12 | 28 | | | | |
| | Right precentral gyrus | 6 | 0.087 | 38 | −8 | 52 | | | | |
| | Left superior frontal gyrus | 6 | 0.218 | −2 | 4 | 48 | | | | |
| Limbic | Left cingulate gyrus | 23 | 0.090 | 0 | −28 | 28 | | | | |
| | | 31 | 0.086 | −2 | −36 | 28 | | | | |
| | Left anterior cingulate | 24 | 0.082 | −4 | 36 | −2 | | | | |
| | Right parahippocampal gyrus | 27 | 0.074 | 24 | −34 | 0 | | | | |
| | | Hippocampus | 0.075 | 26 | −18 | −16 | | | | |
| Midbrain | Right midbrain | Red nucleus | 0.106 | 2 | −24 | 0 | | | | |
| occipital | Left lingual gyrus | | 0.073 | −6 | −80 | 2 | | | | |
| | | 17 | 0.078 | −18 | −86 | 0 | | | | |
| | Left inferior occipital gyrus | 19 | 0.073 | −38 | −70 | −6 | | | | |
| | Right inferior temporal gyrus | 37 | 0.082 | 42 | −66 | −2 | | | | |
| Parietal | Left postcentral gyrus | 2 | 0.104 | −42 | −30 | 52 | | | | |
| | | 2 | 0.074 | −48 | −26 | 32 | | | | |
| | | 2 | 0.072 | −46 | −24 | 38 | | | | |
| | Left inferior parietal lobule | 7 | 0.147 | −30 | −56 | 42 | | | | |
| | Right inferior parietal lobule | 40 | 0.114 | 34 | −46 | 42 | | | | |
| | Right supramarginal gyrus | 40 | 0.083 | 52 | −46 | 32 | | | | |
| | Right superior parietal lobule | 7 | 0.086 | 22 | −66 | 46 | | | | |
| | | 7 | 0.085 | 26 | −62 | 40 | | | | |
| Posterior | Left declive | | 0.083 | −6 | −74 | −18 | | | | |
| | Right declive of vermis | | 0.072 | 2 | −68 | −22 | | | | |
| Sub-lobar | Right caudate | Caudate head | 0.260 | 10 | 8 | 2 | | | | |
| Temporal | Left superior temporal gyrus | 22 | 0.084 | −50 | −16 | 6 | | | | |
| | | 22 | 0.095 | 50 | −10 | 0 | | | | |
| | | 22 | 0.092 | −52 | −40 | 10 | | | | |
| | Right superior temporal gyrus | 22 | 0.086 | 52 | −32 | 6 | | | | |
| | Left fusiform gyrus | 37 | 0.120 | −42 | −58 | −16 | | | | |
| Frontal | Left middle frontal gyrus | 9 | | | | | 0.057 | −42 | 24 | 28 |
| | Right middle frontal gyrus | 6 | | | | | 0.055 | 42 | 0 | 46 |
| | | 10 | | | | | 0.052 | 32 | 46 | 18 |
| | Left superior frontal gyrus | 10 | | | | | 0.039 | −26 | 52 | −2 |
| | Left medial frontal gyrus | 6 | | | | | 0.062 | 0 | −6 | 62 |
| | | 32 | | | | | 0.113 | −2 | 8 | 44 |
| | Left precentral gyrus | 4 | | | | | 0.039 | −40 | −14 | 50 |
| | Left inferior frontal gyrus | 44 | | | | | 0.081 | −50 | 6 | 18 |
| | Right cingulate gyrus | 32 | | | | | 0.101 | 2 | 20 | 34 |
| Limbic | Right anterior cingulate | 32 | | | | | 0.046 | 2 | 46 | 2 |
| | Left cingulate gyrus | 32 | | | | | 0.104 | −2 | 16 | 40 |
| Parietal | Left superior parietal lobule | 7 | | | | | 0.066 | −26 | −62 | 44 |
| Sub-lobar | Right caudate | Caudate body | | | | | 0.322 | 12 | 8 | 8 |
| | Right lentiform nucleus | Lateral globus pallidus | | | | | 0.041 | 20 | −4 | −8 |
| | Right thalamus | Pulvinar | | | | | 0.047 | 6 | −30 | 2 |
| Temporal | Left middle temporal gyrus | 37 | | | | | 0.046 | −48 | −54 | −2 |

Given that we also ran MACM analyses within each behavioral domain to develop domain specific functional connectivity maps (results below), we also performed a post-hoc $\chi^2$ test on the distribution resulting from bilateral caudate ROIs input into each of the BrainMap behavioral domains to ensure that the ALE results were indeed indicative of that particular behavioral domain. We found that for bilateral

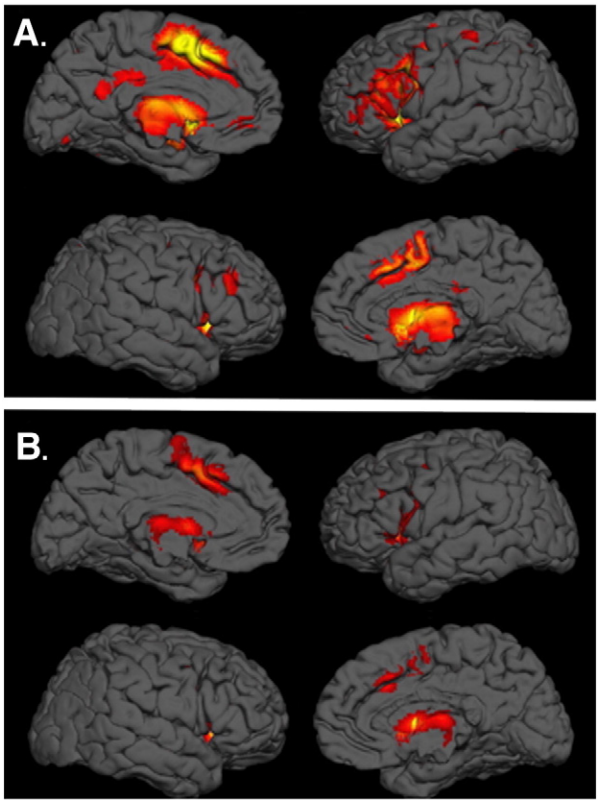


**Fig. 1.** Meta-analytic connectivity models of the human caudate. functional connectivity maps of the left (A) and right (B) caudate nucleus.

caudate results in the domain of action, a higher than expected distribution was found in action ($p<0.0001$), and lower than expect frequencies were found in cognition ($p<0.0001$) and emotion ($p<0.0001$). For cognition, we found lower frequency distributions for action ($p<0.0001$), interoception ($p<0.0003$), and perception ($p<0.0001$), but higher distributions for both cognition ($p<0.0001$) and emotion ($p<0.0001$). For emotion, we found lower than expected distributions for action ($p<0.0001$), cognition ($p<0.0009$), and perception ($p<0.0001$), and a higher distribution than expected in emotion ($p<0.0001$). Finally, for perception, we found lower than expected distributions in cognition ($p<0.0001$) and emotion ($p<0.0000$), and higher than expected in perception ($p<0.0001$). These data provide evidence for the specificity of the functional connectivity maps generated by behavioral-filtering, with only the cognition-specific based $\chi^2$ analysis showing significant overlap between two behavioral domains (emotion and cognition).

*Behavioral filtering analyses*

The second analysis strategy was to create behavior domain specific MACM maps. We used identical MACM methods as described above, however, instead of seeding the caudate ROIs into the entire database, we seeded them into each of the behavioral domains to generate a functional connectivity map for each domain. To identify regions of connectivity that were specific to each behavioral domain, we created a binary cumulative mask of all behavioral domain maps, and simply subtracted all but one binary behavioral domain mask from the cumulative map (e.g., to create the action-specific mask, we subtracted emotion, cognition, and perception from the cumulative mask). This eliminated regions that were involved in more than one domain. Results demonstrated behavioral-domain specific regions of coactivation were consistent with neurological expectations. For example, there were action-specific clusters noted in the postcentral gyrus and putamen; cognition specific clusters in the posterior cingulate, anterior cingulate, and parahippocampal gyrus; and emotion specific clusters in the amygdala, anterior cingulate, and inferior frontal gyrus (Table 2; Fig. 2).

While specificity was demonstrated, we also noted extensive overlap among the behavioral domain networks. For example, the left inferior frontal gyrus (BA47), cingulate gyrus (BA32), and right middle frontal gyrus (BA46) were found to be coactivated with the

**Table 2**
Regions that demonstrated functional connectivity to the caudate within only one behavioral domain.

| Lobe | x | y | z | Description | BA |
|---|---|---|---|---|---|
| *Action specific clusters* | | | | | |
| Anterior | 4 | −58 | −18 | Right culmen | |
| | −16 | −58 | −20 | Left dentate | |
| | 18 | −52 | −22 | Right dentate | |
| Frontal | −52 | −14 | 40 | Left postcentral gyrus | 4 |
| | 0 | −4 | 56 | Left medial frontal gyrus | 6 |
| | −40 | 26 | 26 | Left middle frontal gyrus | 9 |
| | 48 | 6 | 16 | Right inferior frontal gyrus | 44 |
| Parietal | −48 | −26 | 28 | Left postcentral gyrus | 2 |
| | −34 | −28 | 50 | Left postcentral gyrus | 3 |
| | −20 | −66 | 46 | Left precuneus | 7 |
| | −14 | −76 | 36 | | |
| Temporal | −40 | −30 | 16 | Left superior temporal gyrus | 41 |
| | 48 | −26 | 18 | Right superior temporal gyrus | 41 |
| | −58 | −30 | 12 | Left superior temporal gyrus | 42 |
| | 60 | −20 | 12 | right superior temporal gyrus | 42 |
| Sub-lobar | 24 | −2 | 6 | Right putamen | |
| | 10 | −14 | −2 | Right subthalamic nucleus | |
| | −14 | −20 | 6 | Left thalamus (ventral posterior medial nucleus) | |
| *Cognition specific clusters* | | | | | |
| Frontal | −48 | 8 | 26 | Left inferior frontal gyrus | 9 |
| | −2 | 10 | 46 | Left medial frontal gyrus | 32 |
| | −44 | 24 | 22 | Left middle frontal gyrus | 46 |
| | −44 | 42 | 0 | Left inferior frontal gyrus | |
| Limbic | 0 | −50 | 22 | Left posterior cingulate | 30 |
| | 22 | −16 | −10 | Right parahippocampal gyrus | 35 |
| | 0 | 46 | 0 | Right anterior cingulate | |
| Parietal | −36 | −46 | 36 | Left supramarginal gyrus | 40 |
| Posterior | −38 | −58 | −16 | Left declive | |
| Temporal | −56 | −26 | 2 | Left superior Temporal gyrus | 22 |
| | 50 | −28 | 4 | | |
| | 54 | −16 | 2 | | |
| | −50 | −54 | −6 | Left inferior Temporal gyrus | 37 |
| Sub-lobar | −4 | −16 | −8 | Left red nucleus | |
| *Emotion specific clusters* | | | | | |
| Frontal | −44 | 22 | 16 | Left inferior frontal gyrus | 45 |
| | −44 | 30 | 6 | Left inferior frontal gyrus | 46 |
| | 42 | 28 | 12 | Right inferior frontal gyrus | 46 |
| Limbic | 0 | −52 | 22 | Left posterior cingulate | 23 |
| | 0 | 2 | 46 | Left cingulate gyrus | 24 |
| | −24 | −26 | −6 | Left parahippocampal gyrus | 28 |
| | −2 | −36 | 28 | Left cingulate gyrus | 31 |
| | −2 | 48 | −2 | Left anterior cingulate | 32 |
| | −12 | 40 | −2 | Left anterior cingulate | |
| | 22 | −4 | −10 | Right amygdala | |
| Sub-lobar | −30 | 20 | 2 | Left claustrum | |
| | −2 | −14 | −6 | Left mammillary Body | |
| *Perception specific clusters* | | | | | |
| Frontal | −4 | 8 | 48 | Left superior frontal gyrus | 6 |
| | 2 | −2 | 58 | Right medial frontal gyrus | 6 |
| | −56 | 6 | 6 | Left precentral gyrus | 44 |
| | −46 | 4 | 18 | Left inferior frontal gyrus | 44 |
| Parietal | 10 | −74 | 40 | Right precuneus | 7 |
| | −52 | −22 | 16 | Left postcentral gyrus | 40 |
| | 54 | −24 | 22 | Right postcentral gyrus | 40 |
| | −56 | −10 | 16 | Left postcentral gyrus | 43 |
| Posterior | 0 | −70 | −24 | Left tuber of Vermis | |
| Temporal | −46 | −52 | 4 | Left middle temporal gyrus | 37 |
| Sub-lobar | −22 | −4 | −8 | Left lateral globus pallidus | |
| | 10 | −14 | 12 | Right thalamus (medial dorsal nucleus) | |

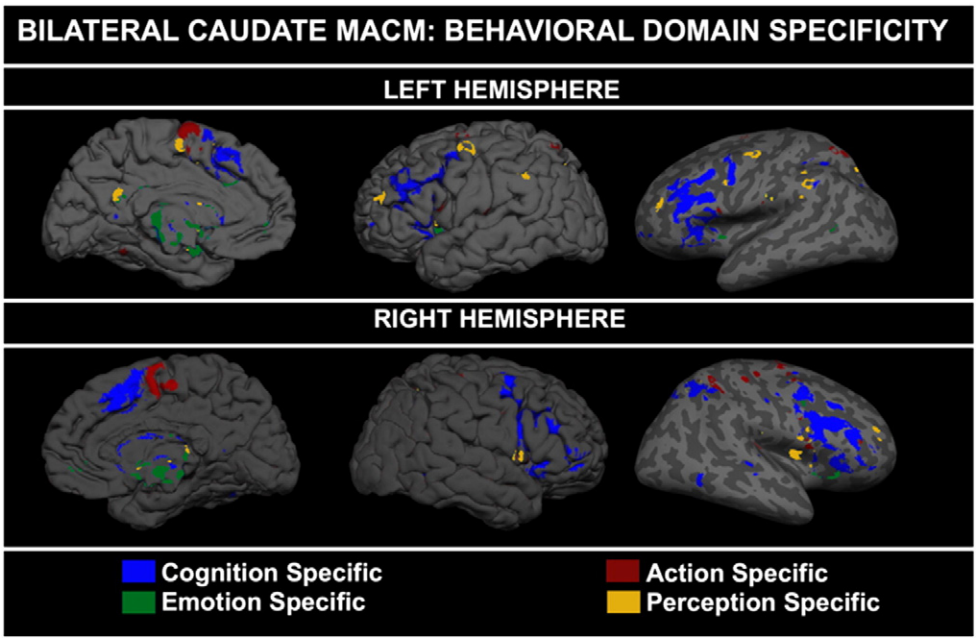


**Fig. 2.** Behavioral domain specific functional connectivity. Maps were generated by binarizing a cumulative connectivity map and subtracting each binarized behavioral domain specific map from the cumulative map (with the exception of the behavioral domain of interest). For example, the cognitive-specific map was created by subtracting the emotion-specific, perception-specific, and action-specific maps from a binarized map of the four domains together.

caudate during cognitive and emotive tasks, while the right precentral gyrus (BA6), right middle frontal gyrus (BA6), right superior parietal lobule (BA7), and left lingual gyrus (BA18) were associated with action and perception tasks (Table 3). Some regions were coactivated across all domains, suggesting a critical connection with the caudate. These regions included bilateral insula (BA13) and the right middle frontal gyrus (BA9) (Fig. 3). The foci of the cluster of activation within the caudate for emotion and cognition were found in the head of the caudate, while the foci coordinates for action and perception mapped to the body of the caudate nucleus, further supporting a topographical organization.

*Head versus body MACM functional connectivity*

A useful demarcation of the caudate nucleus can be made based on observations that the head of the caudate nucleus is more involved in cognitive and emotional processes compared to the body and tail, which have been associated with more action-based processes. Our initial behavioral domain analysis supports this segmentation with emotion and cognition sharing a cluster of activation within the head of the caudate nucleus, while action and perception share a focus within the body of the caudate nucleus. We ran a complementary analysis using a caudate head ROI and a caudate body ROI to develop a MACM for these regions. We created a cumulative, binary mask, and proceeded to subtract the head or the tail connectivity maps to obtain specificity maps. Results showed consistent patterns of behavioral specificity with the head of the caudate having specific functional connectivity with emotive and cognitive regions including the amygdala and portions of the anterior and posterior cingulate (BA32 and 31, respectively) (Fig. 4). The posterior portion of the caudate showed functional connectivity specificity with regions involved in motor control (superior and medial frontal gyri including BA6 and BA8), and perception related processes (occipital clusters were demonstrated as well as regions in the parietal lobe and the posterior cingulate), providing further evidence for a topographic organization. These results should be viewed as preliminary, given that these are not formal statistical comparisons between the head and the tail connectivity maps.

*Anatomical connectivity: topographic organization of the caudate*

To further delineate the anatomical contributions to the proposed segmentation of the caudate nucleus, we performed a DTI analysis using cortical and selected subcortical targets. We found projections to the precentral gyrus, parietal lobe, and postcentral gyrus to be strongest in the posterior portion of the caudate (Figs. 5, Panels B, C, and E respectively). We found strong caudate head projections to the prefrontal cortex (Fig. 5, Panel A), but not the amygdala as we hypothesized. Furthermore, many of the target regions appeared to originate from the central portion of the caudate, embracing elements of both the head and body (e.g., paracingulate, anterior cingulate; Figs. 5, Panels D and G).

At the individual subject level, we found consistent segmentation such that the prefrontal cortex and regions heavily involved in emotion and cognition (i.e., anterior cingulate) had the strongest connectivity in the head portion of the caudate while more action related regions, such as the pre- and postcentral gyri had stronger connectivity in the posterior regions of the caudate. All 49 subjects showed similar segmentation.

*Anatomical connectivity of MACM: validation*

We took the resultant ALE functional connectivity maps for the left and right caudate, and used the cluster foci as targets in a DTI analysis to determine if MACM is identifying nodes of functional connectivity that account for both direct (anatomical) and indirect relations (Fig. 5). 3D-image files containing the output connectivity distribution to the seed masks (left and right caudate independently) were generated for each subject (5000 samples, steplength of 0.5 mm, and curvature threshold of 0.2) using FMRIB's diffusion toolbox (FDT) within the FSL software package (Behrens et al., 2003b; Behrens et al., 2007). Each individual's map was thresholded to >20 samples from each seed voxel to eliminate spurious or low connectivity profiles (Leh et al., 2006; Leh et al., 2007). The results were binarized and summed across subjects. A cumulative DTI connectivity population map was generated (thresholded to show only reconstructed tracts that were present in over 20% of our subjects) and cluster foci were overlaid to determine which foci had anatomical connections (Fig. 6). For the left caudate, we found anatomical support for connections to the ipsilateral superior temporal gyrus (BA22),

**Table 3**
Bilateral caudate ROIs were seeded in each behavioral domain of the BrainMap database to search for regions of coactivation, thus determining behavioral-domain specific functional connectivity. ALE meta-analyses were performed and resultant maps demonstrated overlapping regions of functional connectivity among some brain regions, while others were specific to one behavioral domain (Table 2).

| Caudate functional connectivity: shared clusters across behavioral domains | | | | | | | | | | | | | | |
|---|---|---|---|---|---|---|---|---|---|---|---|---|---|---|
| Lobe | Action | | | Cognition | | | Emotion | | | Perception | | | Description | BA |
| | x | y | z | x | y | z | x | y | z | x | y | z | | |
| Frontal | −36 | −4 | 46 | −30 | −4 | 56 | | | | −26 | −10 | 56 | Left middle frontal gyrus | 6 |
| | −50 | 2 | 30 | −42 | −2 | 44 | | | | | | | Left precentral gyrus | 6 |
| | −26 | −12 | 56 | | | | | | | | | | | |
| | 24 | −14 | 50 | | | | | | | 38 | 2 | 30 | Right precentral gyrus | 6 |
| | 38 | −10 | 52 | | | | | | | 38 | −10 | 52 | | |
| | 24 | −8 | 62 | | | | | | | 26 | −8 | 60 | Right middle frontal gyrus | 6 |
| | 32 | −8 | 44 | | | | | | | | | | | |
| | 38 | 0 | 44 | | | | | | | | | | | |
| | 40 | 32 | 32 | 42 | 32 | 32 | 32 | 34 | 28 | 40 | 32 | 32 | Right middle frontal gyrus | 6 |
| | | | | 44 | 8 | 32 | | | | | | | | |
| | | | | 34 | 30 | 30 | | | | | | | | |
| | | | | 32 | 54 | 6 | | | | | | | Right middle frontal gyrus | 9 |
| | | | | 36 | 46 | 18 | | | | 34 | 46 | 18 | | |
| | | | | 42 | 30 | 12 | 46 | 22 | 22 | | | | Right middle frontal gyrus | 46 |
| | | | | −46 | 20 | 2 | −46 | 18 | 2 | | | | Left inferior frontal gyrus | 47 |
| Limbic | | | | −2 | 20 | 42 | 0 | 22 | 38 | | | | Left cingulate gyrus | 32 |
| Parietal | −30 | −60 | 46 | −30 | −58 | 42 | | | | −32 | −60 | 46 | Left superior parietal lobule | 7 |
| | | | | | | | | | | −24 | −64 | 48 | | |
| | 24 | −66 | 52 | | | | | | | 24 | −66 | 54 | Right superior parietal lobule | 7 |
| | −40 | −34 | 42 | −56 | −42 | 26 | | | | | | | Left inferior parietal lobule | 40 |
| | −34 | −44 | 44 | | | | | | | | | | | |
| | 34 | −42 | 40 | 34 | −48 | 38 | | | | 34 | −46 | 40 | Right inferior parietal lobule | 40 |
| | 52 | −46 | 32 | | | | | | | 52 | −46 | 32 | | |
| Occipital | −12 | −84 | −2 | | | | | | | −12 | −84 | −4 | Left lingual gyrus | 18 |
| Sub-lobar | −46 | 10 | 6 | | | | −40 | 14 | 16 | | | | Left insula | 13 |
| | −30 | 20 | 6 | −32 | 20 | 6 | −38 | −6 | 14 | −34 | 14 | 6 | | |
| | 48 | 12 | 6 | 32 | 20 | 4 | 38 | 18 | 2 | 34 | 18 | 4 | Right insula | 13 |
| | | | | | | | | | | 46 | −24 | 16 | | |
| | | | | | | | | | | 48 | 12 | 6 | | |
| | −14 | 12 | 8 | | | | | | | | | | Left caudate body | |
| | −14 | 0 | 14 | | | | | | | −14 | 0 | 16 | | |
| | 12 | 12 | 10 | | | | | | | | | | Right caudate body | |
| | 12 | 2 | 10 | | | | | | | 12 | 0 | 16 | | |
| | 14 | −6 | 18 | | | | | | | | | | | |
| | | | | −12 | 8 | 4 | −10 | 6 | 2 | | | | Left caudate head | |
| | | | | 10 | 8 | 4 | 10 | 8 | 2 | | | | Right caudate head | |
| | | | | 6 | −20 | −6 | 2 | −22 | −4 | | | | Right red nucleus | |
| | | | | −8 | −18 | 10 | −6 | −16 | 12 | −10 | −16 | 8 | Left thalamus (medial dorsal nucleus) | |
| | 12 | −12 | 14 | 10 | −30 | 0 | | | | | | | | |
| | | | | | | | 2 | −28 | 2 | 16 | −28 | 6 | Right thalamus (pulvinar) | |

fusiform gyrus (BA37), inferior occipital gyrus (BA19), lingual gyrus (BA17), the ventral posterior medial and medial nucleus of the thalamus, and the posterior (BA30) and cingulate gyri (BA23/31). We also provide evidence for contralateral connectivity to the right thalamus, superior parietal lobule (BA7), the parahippocampus (BA27) and hippocampus, as well as the superior temporal gyrus (BA22). For the right caudate, we found ipsilateral connectivity to the lentiform nucleus (lateral globus pallidus), the pulvinar, and the insula (BA13). Contralateral connectivity was identified with the inferior temporal gyrus (BA37), medial dorsal nucleus of the thalamus, and the posterior cingulate (BA31). Many of the foci identified by MACM did not appear to have direct connectivity, suggesting that MACM is identifying nodes with both direct and indirect influence from the caudate.

## Discussion

Our results provide strong evidence for a behavior-based topographic organization previously suggested by histological and functional imaging studies, while also demonstrating the utility of using MACM to develop models of functional connectivity that account for both direct and indirect influences. Below, we discuss these differences in the context of their categorical influences.

### *Direct influences on caudate functional connectivity patterns: diffusion tensor imaging*

This is the first study to combine MACM with DTI processing in a large sample of healthy individuals. We interrogated DTI data with two primary purposes. First, we wanted to identify anatomical pathways that would provide support for direct (i.e., monosynaptic) neural influences of the caudate nucleus on other regions of the brain. Second, we wanted to determine if topographical organization of the caudate nucleus is supported in humans. The latter will be discussed in Section 4.3.

Using a population tractography approach, we provide monosynaptic connectivity evidence supporting components of previously described circuits that were also identified by MACM. Specifically, we found anatomical connectivity between the caudate and the posterior cingulate and cingulate gyri (BA23/30/31), the parahippocampus, and the hippocampus, which are all regions of the brain considered to be part of the emotion-cognition integrative system (Pessoa, 2008) (Fig. 6). We also found monosynaptic connectivity to regions of visual processing such as the fusiform gyrus (BA37) and inferior occipital gyrus (BA19). The superior (BA22) and inferior temporal gyri also demonstrated direct connectivity with the caudate. Furthermore, we found anatomical connectivity between the caudate and different nuclei of the

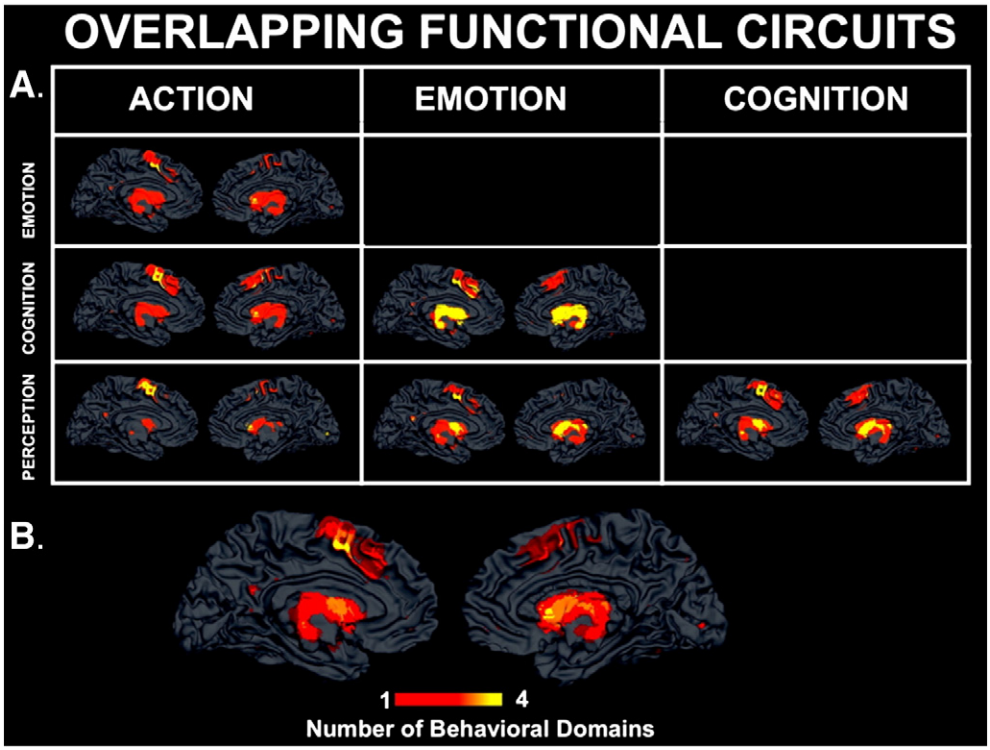


**Fig. 3.** Behavioral domain connectivity maps. A. MACM behavioral domain results demonstrating overlapping functional circuits across behavioral domains. Yellow indicates overlap, whereas red indicates only one of the two behavioral domains utilizes the region. B. Cumulative MACM behavioral domain map demonstrating the number of behavioral domains using each region. Dark red indicates a more specific node (i.e., only one behavioral domain mapped to the region) in the circuit, whereas yellow represents a less domain specific component of the circuit (i.e., all behavioral domain networks access the region). Interoception and pharmacology did not have enough papers entered into the database, and thus lacked power, to be included in these analyses.

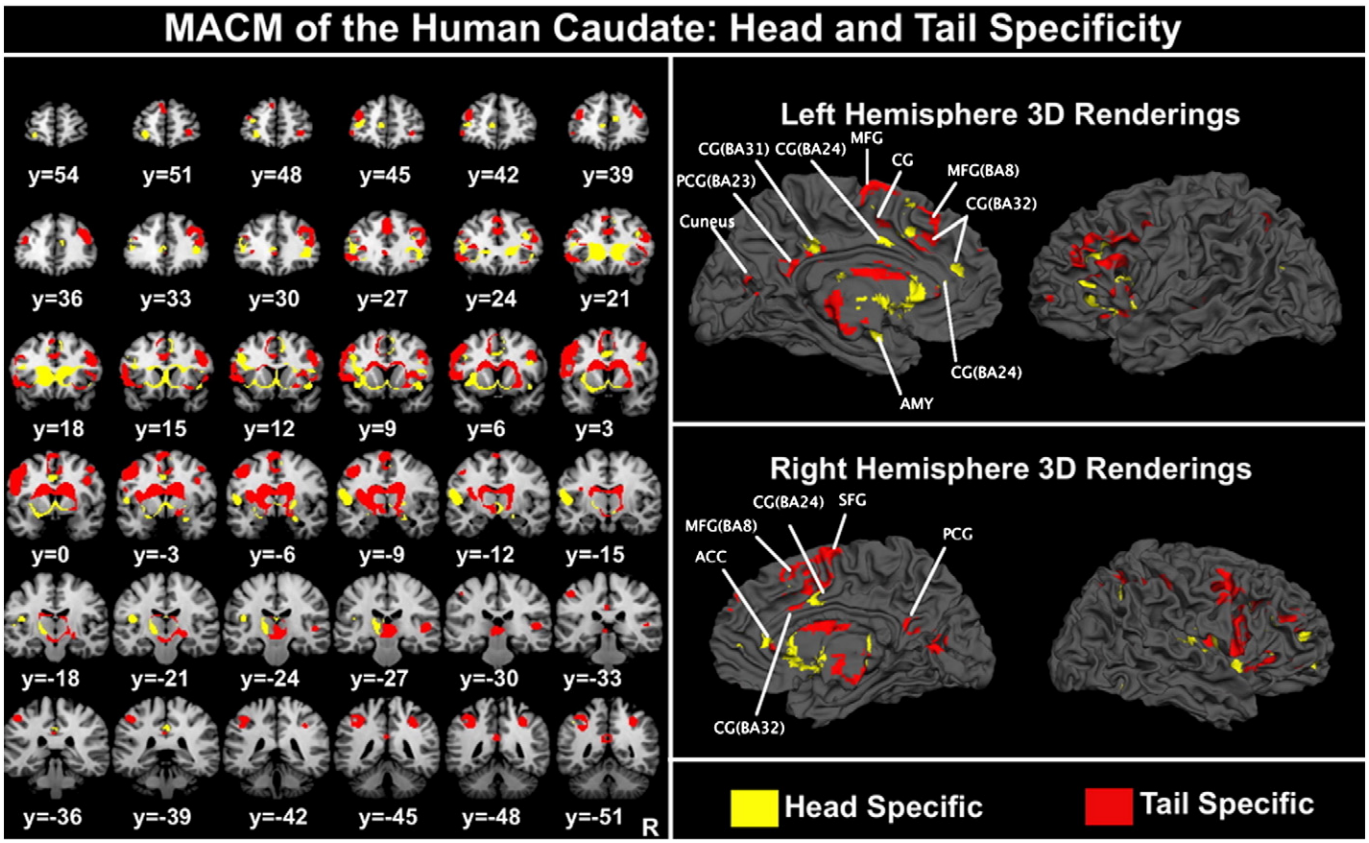


**Fig. 4.** Differentiating topographic network organization using MACM. After manual segmentation based on previous research, functional connectivity differences were noted between the connectivity maps generated for the head (in yellow) and the body (in red) of the caudate.

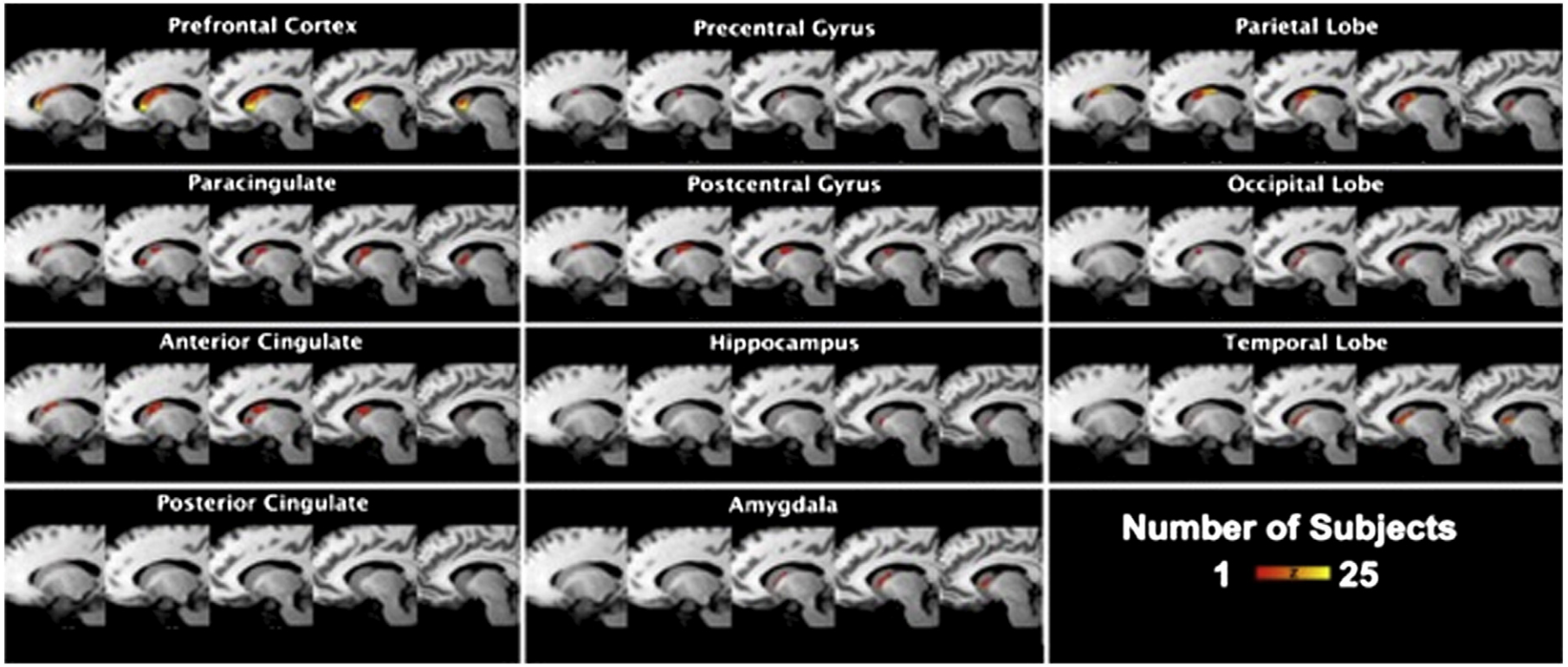


**Fig. 5.** DTI of the human caudate. For each cortical and subcortical target, we thresholded and binarized individual subject results to include only those caudate voxels with a connection probability > 10%. These images were summed across subjects to generate a population map reflecting anatomical caudate segmentation. Slices shown from left to right are x = −15, −13, −11, −9, and −7.

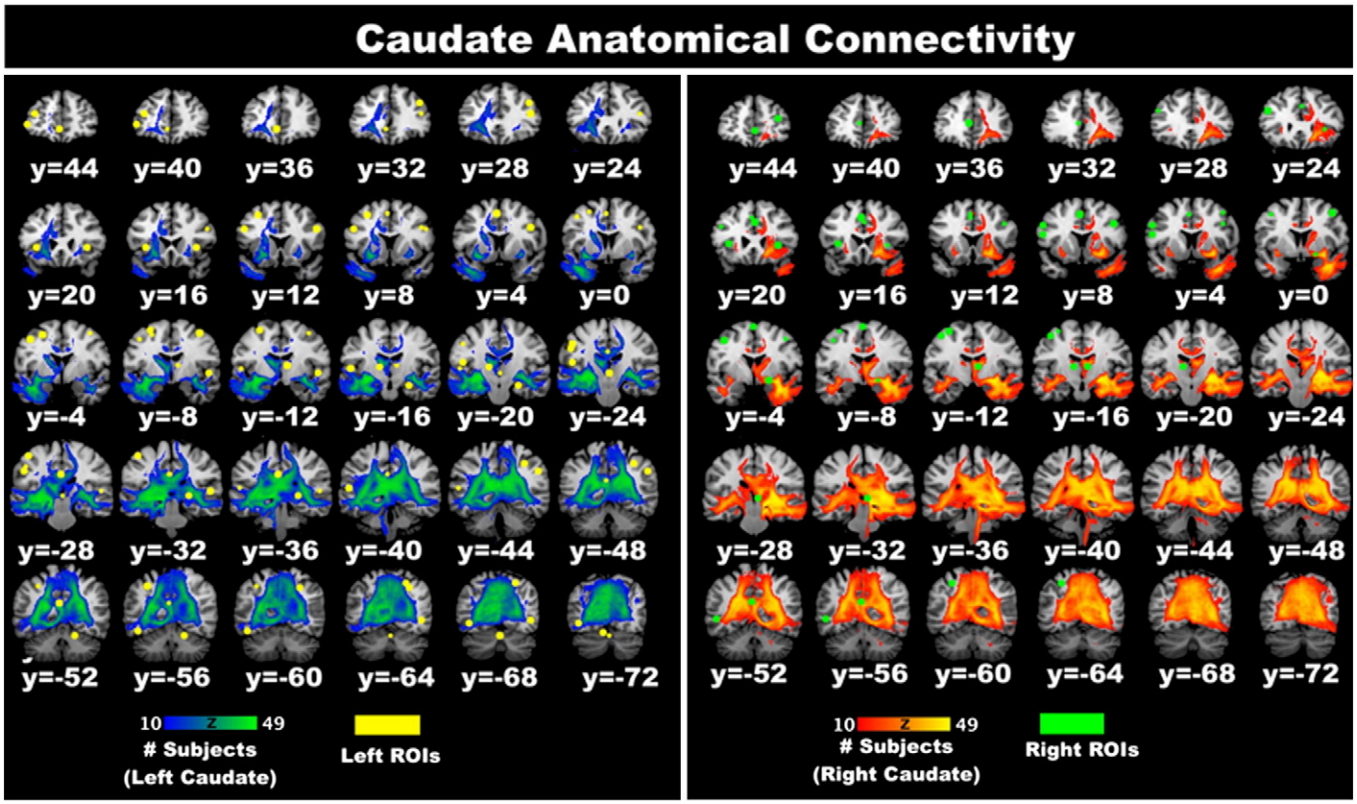


**Fig. 6.** MACM and DTI convergence and divergence. Cumulative DTI connectivity distributions with right caudate ALE cluster foci in solid green, and tracts red-yellow. Left caudate tracts are in blue-green with solid yellow representing the left caudate MACM foci. Several foci did did not have anatomical support as indicated by a lack of tractography to the foci node.

thalamus (i.e., pulvinar, medial dorsal nucleus) supporting the long-standing notion that the thalamus provides critical operations that require such architecture for efficiency. This latter connection appears to be the most prominently replicated across studies (Leh et al., 2007).

Our results deviate slightly from other research findings regarding anatomical connectivity of the human caudate. For example, Lehericy et al. (2004) studied 9 individuals and found corticostriatal connections primarily within the frontal cortex. Their results suggest that fibers associated with the head of the caudate nucleus are directed toward the medial, dorsal (BA9/46) and ventral (BA45/47) prefrontal cortices. Similarly, Leh et al. (2007) studied 6 individuals and found caudate projections to the ipsilateral prefrontal cortex, middle and inferior temporal gyrus, frontal eye fields, cerebellum, and thalamus. Though our results parallel some of these connections (inferior temporal gyrus and thalamus), they do not provide the same anatomical support for the prefrontal regions. This difference may be explained by our thresholding, or by the boundaries of our ROIs. We determined monosynaptic connectivity only to the ROIs within these regions that were identified by MACM analyses. Thus, the entire region was not considered for direct influence, rather a 5 mm sphere generated around each caudate MACM foci.

DTI studies are often criticized for their inability to provide direct information about functional networks (Di Martino et al., 2008). Combining MACM and DTI provides a solution to this issue by elucidating white matter connectivity to ROIs established within functional circuits. Here, we demonstrate how this technique can be used to inform the monosynaptic versus polysynaptic (i.e., indirect) architecture of connectivity models.

### *Indirect influences on caudate functional connectivity: support from meta-analytic connectivity modeling*

Many of the nodes identified by MACM were not supported by our anatomical analyses. These regions were primarily within networks subserving emotion and cognition including the anterior cingulate (BA24/32), prefrontal regions (BA9/46), and insula (BA13). However, portions of the motor (i.e., precentral gyrus [BA6]) and perceptual (i.e., inferior parietal lobule [BA40]) networks were also noted as having polysynaptic influence. These results are supported by other studies noting functional connectivity of the striatum during the resting state (Di Martino et al., 2008). Specifically, Di Martino et al. (2008) demonstrated positive coherence between the ventromedial caudate and portions of the orbitofrontal cortex (BA10), dorsolateral prefrontal cortex (BA9), inferior frontal gyrus (BA47), and the anterior cingulate (BA32). Interestingly, they did not find positive coactivations with the parahippocampus or the posterior cingulate as we did. Furthermore, their connectivity analyses revealed negative correlations between the dorsal caudate and the posterior cingulate, portions of the occipital cortex, and the cerebellum. Another resting state study corroborated these negative correlations (Barnes et al., 2010), suggesting that some regions identified by MACM, which only identifies regions of coactivation and not deactivations, may be task-dependent hubs, coming online to serve specific processes. Alternatively, it is possible that using different settings for ALE, or using the most refined version may yield these hubs (Eickhoff et al., 2011a; Turkeltaub et al., 2012).

### *Topographical organization of the human caudate*

Nonhuman primate research has suggested a specific organization of the caudate nucleus based on evidence from both anatomical and functional segmentation. For example, Levy et al. (1997) proposed a topographic segmentation derived from physiological and lesion studies (Divac et al., 1967; Rolls, 1994), and subsequently demonstrated such organization using spatial and nonspatial working memory tasks. They found that a delayed spatial alternation task activated the head of the caudate, which is heavily innervated by dorsolateral

prefrontal cortex efferent fibers in the nonhuman primate. Alternatively, a delayed object alternation task activated the body/tail of the caudate, innervated primarily by temporal cortex fibers. This topographic organization has been suggested in human studies (Draganski et al., 2008; Leh et al., 2007; Lehericy et al., 2004).

Using several predefined cortical targets, we used DTI to project where tracts from specific brain regions terminated within the caudate (Fig. 5). We found support for a head/body topographical organization in which emotion and cognitive regions projected mostly to the head of the caudate, and action and perception regions projected close to the posterior portions of the caudate. For example, the prefrontal cortex ROI was largely projecting to the head of the caudate, while the occipital lobe tracts were mostly localized to the ventral body of the caudate.

Researchers have also proposed a slightly different topographical organization of the caudate, with 3 defined functional zones: associative striatum (head of caudate), sensorimotor striatum (dorsolateral rim of the caudate), and the limbic striatum (ventral caudate) (Nakano et al., 2000; Parent and Hazrati, 1995; Postuma and Dagher, 2006; Selemon and Goldman-Rakic, 1988). This has been akin to a dorsal-ventral continuum with a spectrum ranging from cognitive (dorsal) to affective (ventral) control. With regard to these functional zones, we found strong ventral caudate connectivity to the hippocampus and amygdala (Figs. 5, Panel H and Panel K, respectively) from our DTI analysis, supporting the concept of a 'limbic striatum'. Additionally, the temporal lobe demonstrated connectivity to the ventral portion of the caudate nucleus (Fig. 5, Panel I). We also found some support for the sensorimotor striatum with caudate connectivity to the parietal and postcentral gyrus, both spanning the ventral and dorsal portions (Figs. 5, Panel C and E, respectively). Similar connectivity profiles have been suggested. For example, Lehericy et al. (2004) found that tracking from 4 large cortical targets (motor, premotor, prefrontal, and orbitofrontal) yielded prefrontal connections projecting to the head of the caudate nucleus. Similarly, Leh et al. (2007) found connections with the dorsolateral prefrontal cortex and the dorsal-posterior caudate, as well as ventrolateral prefrontal cortex projections to the ventral-anterior portion of the caudate, while Draganski et al. (2008) found that the dorsolateral prefrontal cortex diffusely connected to the rostral and caudal components of the caudate. Our results parallel these findings, but with less specificity (i.e., ventral and dorsal prefrontal cortices) in comparison to previous studies because of our chosen cortical targets.

In comparison to the nonhuman primate literature, our results are highly concordant. The associative striatum primarily occupies the head of the caudate nucleus where it receives afferent connections from a variety of cortical areas. Area 46 projects to the head of the caudate nucleus, and Area 9 localizes to the intermediate part of the caudate nucleus, with projections denser ventrally in the nonhuman primate (Nakano, 2000; Nakano et al., 2000). This is identical to what we demonstrate in the human (Fig. 5, Panel A). The limbic striatum occupies the central portion of the caudate nucleus, much like in our study (Fig. 5, Panels G, H, I, K) (Nakano, 2000; Nakano et al., 2000).

### *BrainMap database and ALE*

The BrainMap database has proven to be an invaluable tool for data mining and developing models of functional connectivity. Here, we have capitalized on the rigorous coding scheme outlined and validated in previous publications (Fox et al., 2005; Laird et al., 2009a,b; Laird et al., 2011a,b), and available at the BrainMap website (http://www.brainmap.org/BrainMapLex.xls). Our data support functional segregation of the human caudate. Results strengthen previous studies, which found high concordance of the database coding structure to known intrinsic and task-related networks (Eickhoff et al., 2011b; Kurth et al., 2010; Laird et al., 2009b, 2011b; Smith et al., 2009).

We do note that there are limitations to the use of MACM, and ALE, to develop models of functional connectivity. First, results may be influenced by the user-specified criteria within the ALE program (i.e., false discovery rate, minimum cluster size), and by the thresholding of the initial ROIs used for the analysis. This latter point seems to have minimal effects, as noted in Robinson et al.'s (2010) study of the amygdala. There are also minor statistical disadvantages to the ALE algorithm used in the above analyses (i.e., within-group and within-experiment effects on ALE values, a potential underestimation of the right-tail of the null distribution of the random spatial association between experiments, and lack of family-wise error correction) (Eickhoff et al., 2011a; Turkeltaub et al., 2012). Most of these issues have been resolved with a refined ALE algorithm that is now available (Eickhoff et al., 2011a). However, the selection and thresholding of target ROIs for inclusion in DTI analyses may have a more pronounced effect on the results, and thus should be rationally considered. To date, there is no guide for these type of analyses, and the selection and thresholding has varied across studies, with the majority using very large target ROIs, despite these targets having documented functional segmentations (Behrens et al., 2003b; Johansen-Berg et al., 2004, 2005). We chose to break these large targets into smaller ROIs with probability maps associated with them. As more studies utilize this technique, we'll better understand what differences these subjective choices make on results.

### *Conclusions*

MACM results were consistent with previous studies examining coactivation patterns with the caudate (Acheson et al., 2009; Bluhm et al., 2009; Blumberg et al., 2000; Postuma and Dagher, 2006). However, our study represents a more robust analysis allowing for the detection of an extensive functional connectivity network that has additional nodes not previously identified by individual studies. We also corroborate evidence supporting connectivity with regions such as the anterior cingulate which, when lesioned, has been shown to reduce the volume of the caudate nucleus (Rauch et al., 2000). Other MACM studies have consistently shown high coherence with the functional neuroimaging literature as well (Cauda et al., 2011; Robinson et al., 2010). Furthermore, our structural and MACM analyses together demonstrate strong support for functional and anatomical segmentation of the caudate nucleus such that the head of the caudate corresponds closely to cognitive and emotional circuits, and the body or posterior portion of the caudate shows a strong link to action and perception related networks.

Finally, nonhuman primate models have dominated the literature for decades, and as such, have also evolved over the years. Alexander et al. (1986) proposed the existence of 5 parallel functional looping circuits, while others have proposed that the caudate is composed of 3 functional zones: associative striatum (head of caudate), sensorimotor striatum (dorsolateral rim of the caudate), and the limbic striatum (ventral caudate) (Nakano et al., 2000; Parent and Hazrati, 1995; Postuma and Dagher, 2006; Selemon and Goldman-Rakic, 1988). Our data provide support for 3 of the 5 domain-specific circuits proposed by Alexander and colleagues (Alexander et al., 1986). Specifically, the prefrontal, motor, and anterior cingulate circuits were identified in our data. The prefrontal looping circuit is evidenced by the present observations of cognition-specific regions of coactivation with the caudate; the motor loop is represented by identical cortical targets; and the anterior cingulate/limbic loop is similar to our emotion-specific circuit. In addition to support for these circuits, our data allow us to make additional observations. For example, our human-based cognition specific circuit was more expansive and included more medial regions than in the primate models (i.e., cingulate). Our emotion circuit contained distinct caudate coactivations in the amygdala and part of the hippocampus, in addition to the prefrontal region. In summary, MACM results shows strong support for

existing primate models, while also providing additional insight into human-specific divergent circuitry.

The human caudate has been implicated in a variety of neurological and psychiatric disorders. Identifying a comprehensive model of functional connectivity may help elucidate the pathophysiological mechanisms underlying these disorders. Furthermore, our data demonstrate that using MACM in combination with DTI methodology may aid in parsing direct from indirect influences, which may ultimately strengthen models of disease. To our knowledge, this is the first study aimed at developing a robust model of the human caudate using MACM, and supplemented with DTI analyses. Future research should examine MACM based functional connectivity models using structural equation modeling (SEM) of healthy and diseased populations with known deficits in the given structure of interest. The use of MACM-derived models should provide improved initial models for SEM and other path analysis techniques. Thus, MACM provides a sturdy foundation for connectivity analyses that may ultimately lead to an improvement in our understanding of healthy cognition and disease pathology. Finally, MACM may be used to compare connectivity patterns that emerge in task-independent functional imaging (i.e., resting state fMRI), during which the default mode network is most robust, and task-dependent connectivity. Combined with the flexibility to identify behavioral domain specific networks, this could advance our understanding of how networks transition as they are recruited for neural processes.

In summary, our study provides additional evidence of the robust utility of MACM. In a recent study, Cauda et al. (2011) found high correlations between MACM and resting state fMRI data of the nucleus accumbens. Here, we have demonstrated similar consistency of MACM data with existing fMRI and PET studies of the caudate. Capitalizing on the organizational structure of the BrainMap database (Fox and Lancaster, 2002; Fox et al., 2005; Laird et al., 2005b; Laird et al., 2009a), we demonstrate an expanded effectiveness of MACM analyses to elucidate human neural networks specific to behavioral domains. Lastly, we illustrate that when coupled with DTI analysis, MACM can be paired with probabilistic tracking to begin to investigate indirect versus direct influences.

## Conflict of interest

All authors report having no financial, personal, or organizational conflict of interest with the work outlined in this manuscript.

## Acknowledgments

This work was supported by the following grants: NIMH R01-MH074457 (PIs: PTF and ARL), NIMH R01-MH0708143 (PI: DCG), NIMH R01-MH078111 (PI: JB), and NIMH R01-MH083824 (PI: DCG).

## References

Acheson, A., Robinson, J.L., et al., 2009. Differential activation of the anterior cingulate cortex and caudate nucleus during a gambling simulation in persons with a family history of alcoholism: Studies from the Oklahoma Family Health Patterns Project. Drug Alcohol Depend. 100 (1–2), 17–23.
Alexander, G.E., Crutcher, M.D., 1990. Functional architecture of basal ganglia circuits: neural substrates of parallel processing. Trends Neurosci. 13 (7), 266–271.
Alexander, G.E., DeLong, M.R., et al., 1986. Parallel organization of functionally segregated circuits linking basal ganglia and cortex. Annu. Rev. Neurosci. 9, 357–381.
Barnes, K.A., Cohen, A.L., et al., 2010. Identifying basal ganglia divisions in individuals using resting-state functional connectivity MRI. Front. Syst. Neurosci. 4 (Article 18), 1–9.
Behrens, T.E., Woolrich, M.W., et al., 2003a. Characterization and propagation of uncertainty in diffusion-weighted MR imaging. Magn. Reson. Med. 50 (5), 1077–1088.
Behrens, T.E.J., Johansen-Berg, H., et al., 2003b. Non-invasive mapping of connections between human thalamus and cortex using diffusion imaging. Nat. Neurosci. 6 (7), 750–757.
Behrens, T.E.J., Berg, H.J., et al., 2007. Probabilistic diffusion tractography with multiple fibre orientations: what can we gain? NeuroImage 34 (1), 144–155.
Bluhm, R., Williamson, P., et al., 2009. Resting state default-mode network connectivity in early depression using a seed region-of-interest analysis: decreased connectivity with the caudate nucleus. Psychiatry Clin. Neurosci. 63, 754–761.
Blumberg, H.P., Stern, E., et al., 2000. Increased anterior cingulate and caudate activity in bipolar mania. Biol. Psychiatry 48 (11), 1045–1052.
Bohanna, I., Georgiou-Karistianis, N., et al., 2011. Connectivity-based segmentation of the striatum in Huntington's disease: vulnerability of motor pathways. Neurobiol. Dis. 42 (3), 475–483.
Casey, B.J., Epstein, J.N., et al., 2007. Frontostriatal connectivity and its role in cognitive control in parent–child dyads with ADHD. Am. J. Psychiatry 164 (11), 1729–1736.
Castellanos, F.X., Giedd, J.N., et al., 1994. Quantitative morphology of the caudate nucleus in attention deficit hyperactivity disorder. Am. J. Psychiatry 151 (12), 1791–1796.
Cauda, F., Cavanna, A.E., et al., 2011. Functional connectivity and coactivation of the nucleus accumbens: a combined functional connectivity and structure-based meta-analysis. J. Cogn. Neurosci. 1–14.
DeLong, M.R., Georgopoulos, A.P., et al., 1983. Cortico-basal ganglia relations and coding of motor performance. Exp. Brain Res. Suppl. 7, 30–40.
Di Martino, A., Scheres, A., et al., 2008. Functional connectivity of the human striatum: a resting state fMRI study. Cereb. Cortex 18, 2735–2747.
Divac, I., Rosvold, H.E., et al., 1967. Behavioral effects of selective ablation of the caudate nucleus. J. Comp. Physiol. Psychol. 63 (2), 184–190.
Draganski, B., Kherif, F., et al., 2008. Evidence for segregated and integrative connectivity patterns in the human basal ganglia. J. Neurosci. 28 (28), 7143–7152.
Eickhoff, S.B., Bzdok, D., et al., 2011a. Activation likelihood estimation meta-analysis revisited. NeuroImage (0).
Eickhoff, S.B., Bzdok, D., et al., 2011b. Co-activation patterns distinguish cortical modules, their connectivity and functional differentiation. NeuroImage 57 (3), 938–949.
Fox, P.T., Lancaster, J.L., 2002. Opinion: mapping context and content: the BrainMap model. Nat. Rev. Neurosci. 3 (4), 319–321.
Fox, P.T., Laird, A.R., et al., 2005. BrainMap taxonomy of experimental design: description and evaluation. Hum. Brain Mapp. 25 (1), 185–198.
Gianaros, P.J., Sheu, L.K., et al., 2008. Individual differences in stressor-evoked blood pressure reactivity vary with activation, volume, and functional connectivity of the amygdala. J. Neurosci. 28 (4), 990–999.
Grahn, J.A., Parkinson, J.A., et al., 2008. The cognitive functions of the caudate nucleus. Prog. Neurobiol. 86, 141–155.
Haber, S.N., 2003. The primate basal ganglia: parallel and integrative networks. J. Chem. Neuroanat. 26, 317–330.
Jenkinson, M., Bannister, P., et al., 2002. Improved optimization for the robust and accurate linear registration and motion correction of brain images. NeuroImage 17 (2), 825.
Johansen-Berg, H., Behrens, T.E., et al., 2004. Changes in connectivity profiles define functionally distinct regions in human medial frontal cortex. Proc. Natl. Acad. Sci. U. S. A. 101 (36), 13335–13340.
Johansen-Berg, H., Behrens, T.E., et al., 2005. Functional–anatomical validation and individual variation of diffusion tractography-based segmentation of the human thalamus. Cereb. Cortex 15, 31–39.
Kurth, F., Zilles, K., et al., 2010. A link between the systems: functional differentiation and integration within the human insula revealed by meta-analysis. Brain Struct. Funct. 214 (5), 519–534.
Laird, A.R., Fox, P.M., et al., 2005a. ALE meta-analysis: controlling the false discovery rate and performing statistical contrasts. Hum. Brain Mapp. 25 (1), 155–164.
Laird, A.R., Lancaster, J.L., et al., 2005b. BrainMap: the social evolution of a human brain mapping database. Neuroinformatics 3 (1), 65–78.
Laird, A.R., Eickhoff, S.B., et al., 2009a. ALE meta-analysis workflows via the BrainMap database: progress towards a probabilistic functional brain atlas. Front. Neuroinformatics 3, 1–11.
Laird, A.R., Eickhoff, S.B., et al., 2009b. Investigating the functional heterogeneity of the default mode network using coordinate-based meta-analytic modeling. J. Neurosci. 29 (46), 14496–14505.
Laird, A., Eickhoff, S., et al., 2011a. The BrainMap strategy for standardization, sharing, and meta-analysis of neuroimaging data. BMC Res. Notes 4, 349. doi:10.1186/1756-0500-4-349 (1%M).
Laird, A.R., Fox, P.M., et al., 2011b. Behavioral interpretations of intrinsic connectivity networks. J. Cogn. Neurosci. 23 (12), 4022–4037.
Leh, S.E., Johansen-Berg, H., et al., 2006. Unconscious vision: new insights into the neuronal correlate of blindsight using diffusion tractography. Brain 129, 1822–1832.
Leh, S.E., Ptito, A., et al., 2007. Fronto-striatal connections in the human brain: a probabilistic diffusion tractography study. Neurosci. Lett. 419, 113–118.
Lehericy, S., Ducros, M., et al., 2004. Diffusion tensor fiber tracking shows distinct corticostriatal circuits in humans. Ann. Neurol. 55, 522–529.
Levy, R., Friedman, H.R., et al., 1997. Differential activation of the caudate nucleus in primates performing spatial and nonspatial working memory tasks. J. Neurosci. 17 (10), 3870–3882.
Ma, N., Liu, Y., et al., 2011. Abnormal brain default-mode network functional connectivity in drug addicts. PLoS One 6 (1), e16560.
Melrose, R.J., Tinaz, S., et al., 2008. Compromised fronto-striatal functioning in HIV: an fMRI investigation of semantic event sequencing. Behav. Brain Res. 188 (2), 337–347.
Mohanty, A., Engels, A.S., et al., 2007. Differential engagement of anterior cingulate cortex subdivisions for cognitive and emotional function. Psychophysiology 44 (3), 343–351.
Nakano, K., 2000. Neural circuits and topographic organization of the basal ganglia and related regions. Brain Dev. 22, S5–S16.
Nakano, K., Kayahara, T., et al., 2000. Neural circuits and functional organization of the striatum. J. Neurol. 247 (Suppl. 5), V1–V15.
Parent, A., Hazrati, L.-N., 1995. Functional anatomy of the basal ganglia. I. The cortico-basal ganglia-thalamo-cortical loop. Brain Res. Rev. 20 (1), 91–127.

Pessoa, L., 2008. On the relationship between emotion and cognition. Nat. Rev. Neurosci. 9 (2), 148.
Postuma, R.B., Dagher, A., 2006. Basal ganglia functional connectivity based on a meta-analysis of 126 positron emission tomography and functional magnetic resonance imaging publications. Cereb. Cortex 16 (10), 1508–1521.
Rauch, S.L., Kim, H., et al., 2000. Volumetric reduction in caudate nucleus following stereotactic lesions of anterior cingulate cortex in humans: a morphometric magnetic resonance imaging study. J. Neurosurg. 93 (6), 1019–1025.
Robinson, J.L., Laird, A.R., et al., 2010. Metaanalytic connectivity modeling: delineating the functional connectivity of the human amygdala. Hum. Brain Mapp. 31 (2), 173–184.
Rolls, E.T., 1994. Neurophysiology and cognitive functions of the striatum. Rev. Neurol. 150 (8–9), 648–660.
Rowe, J.B., Hughes, L., et al., 2008. Parkinson's disease and dopaminergic therapy — differential effects on movement, reward and cognition. Brain 131, 2094–2105.
Selemon, L., Goldman-Rakic, P., 1988. Common cortical and subcortical targets of the dorsolateral prefrontal and posterior parietal cortices in the rhesus monkey: evidence for a distributed neural network subserving spatially guided behavior. J. Neurosci. 8 (11), 4049–4068.
Smith, S.M., 2002. Fast robust automated brain extraction. Hum. Brain Mapp. 17 (3), 143–155.
Smith, S.M., Jenkinson, M., et al., 2004. Advances in functional and structural MR image analysis and implementation as FSL. NeuroImage 23 (Suppl. 1), S208–S219.
Smith, S.M., Fox, P.T., et al., 2009. Correspondence of the brain's functional architecture during activation and rest. Proc. Natl. Acad. Sci. 106 (31), 13040–13045.
Stein, J.L., Wiedholz, L.M., et al., 2007. A validated network of effective amygdala connectivity. NeuroImage 36 (3), 736.
Turkeltaub, P.E., Eden, G.F., et al., 2002. Meta-analysis of the functional neuroanatomy of single-word reading: method and validation. NeuroImage 16 (3, Part 1), 765.
Turkeltaub, P.E., Eickhoff, S.B., et al., 2012. Minimizing within-experiment and within-group effects in activation likelihood estimation meta-analyses. Hum. Brain Mapp. 33 (1), 1–13.
Turner, K., Frost, L., et al., 2006. Atypically diffuse functional connectivity between caudate nuclei and cerebral cortex in autism. Behav. Brain Funct. 2 (1), 34.
Tzourio-Mazoyer, N., Landeau, B., et al., 2002. Automated anatomical labeling of activations in SPM using a macroscopic anatomical parcellation of the MNI MRI single-subject brain. NeuroImage 15 (1), 273.
Williams, P.L., Warwick, R., et al. (Eds.), 1989. Gray's Anatomy. Churchill Livingstone, Edinburgh.
Williams, L.M., Liddell, B.J., et al., 2006. Amygdala-prefrontal dissociation of subliminal and supraliminal fear. Hum. Brain Mapp. 27 (8), 652–661.